Periodic arrays of flux-closure domains in ferroelectric thin films with oxide electrodes

S. Li, , Y. L. Zhu, , Y. J. Wang, , Y. L. Tang, , Y. Liu, , S. R. Zhang, , J. Y. Ma, and , and X. L. Ma

Citation: Appl. Phys. Lett. **111**, 052901 (2017); doi: 10.1063/1.4996232
View online: http://dx.doi.org/10.1063/1.4996232
View Table of Contents: http://aip.scitation.org/toc/apl/111/5
Published by the American Institute of Physics

Periodic arrays of flux-closure domains in ferroelectric thin films with oxide electrodes

S. Li,[1,2] Y. L. Zhu,[1,a)] Y. J. Wang,[1] Y. L. Tang,[1] Y. Liu,[1] S. R. Zhang,[1,2] J. Y. Ma,[1] and X. L. Ma[1,3]

[1]*Shenyang National Laboratory for Materials Science, Institute of Metal Research, Chinese Academy of Sciences, Wenhua Road 72, 110016 Shenyang, China*
[2]*University of Chinese Academy of Sciences, Yuquan Road 19, 100049 Beijing, China*
[3]*School of Materials Science and Engineering, Lanzhou University of Technology, Langongping Road 287, 730050 Lanzhou, China*

(Received 26 April 2017; accepted 21 June 2017; published online 31 July 2017)

Flux-closure domain structures in ferroelectric thin films are considered to have potential applications in electronic devices. It is usually believed that these structures are stabilized by the depolarization field and the contact with electrodes tends to screen the depolarization field and may limit their formation. In this work, the influence of oxide electrodes ($SrRuO_3$ and $La_{0.7}Sr_{0.3}MnO_3$) on the formation of flux-closure domains in $PbTiO_3$ thin films deposited on (110)-oriented $GdScO_3$ substrates by pulsed laser deposition was investigated by Cs-corrected transmission electron microscopy. It is found that periodic flux-closure domain arrays can be stabilized in $PbTiO_3$ films when the top and bottom electrodes are symmetric, while *a*/*c* domains appear when asymmetric electrodes are applied. The influence of asymmetric electrodes on the domain configuration is proposed to have a connection with their different work functions and conductivity types. These results are expected to shed light on understanding the nature of flux-closure domains in ferroelectrics and open some research possibilities, such as the evolution of these structures under external electric fields. *Published by AIP Publishing.* [http://dx.doi.org/10.1063/1.4996232]

Ferroelectrics have attracted much attention because of their application prospects on data storage, ultra-thin capacitors, energy storage, and tunnel junction devices.[1–3] Due to the requirement of device miniaturization, the ferroelectrics are usually applied in the form of thin films which possess abundant domain structures, exotic interfacial phenomena, and peculiar physical properties.[3,4]

Recently, complex topological structures have been observed and studied in ferroelectric films; among them, flux-closure and vortex domain structures are believed to be promising in the next generation data storage devices.[5–7] For example, Tang *et al.* observed flux-closure domain arrays in $PbTiO_3$ (PTO) multilayers separated by $SrTiO_3$ (STO) ultra-thin layers on $GdScO_3$ (GSO) substrates.[8] Later, Yadav *et al.* observed vortex arrays in PTO layers of PTO/STO superlattices grown on $DyScO_3$ substrates.[9] In both cases, it is believed that these topological domains form in ferroelectric layers when an insulating layer of STO and scandate substrates are introduced. Scandate substrates will provide tensile constraints, and the insulating oxides will exert a strong depolarization field on ferroelectric films, both of which are considered as key factors for the formation of flux-closure domains.[8–11] For the realistic and commercial application of ferroelectric films in a device model, however, the interaction of ferroelectric thin films and electrodes is inevitable, which tends to screen the depolarization field and may destroy flux-closure domains. In a recent work, Peters *et al.* found local curling polarization structures and complex flux-closure curling behaviors in PTO layers of Co/PTO/(La,Sr)MnO_3 ferroelectric tunnel junctions, which suggested that the vortex-type structure could exist in the ferroelectric film with electrodes.[12] It is noted that the curling behaviors in the PTO layers are confined. The reason may be that the STO substrate cannot provide a proper strain state, and the metallic top electrode was utilized in their work. To further judge the impact of electrodes on the formation of topological domains, it is essential to investigate the behavior of oxide electrodes.

As have been shown in our previous works,[8] flux-closure arrays have been fabricated in multilayer PTO/STO systems grown on GSO substrates, which can provide a proper strain state under which *c* and *a* domains would compete with each other. We anticipated that it would have the same character in the PTO/electrode systems. Although the role of electrodes in the formation and stabilization of the vortex-type structure is still unclear, many researches strongly hint that the electrodes can indeed affect ferroelectric polarization, domain morphology, and physical properties of ferroelectric films.[13,14] Oxide electrodes usually have one order of magnitude larger screening lengths than metal electrodes.[15] According to previous studies, the larger the screening length is, the stronger the depolarization field will be exerted onto a ferroelectric film.[16]

In this work, PTO films sandwiched by symmetric oxide electrodes were grown on orthorhombic (110) GSO substrates by pulsed laser deposition (PLD) and observed by conventional transmission electron microscopy (TEM) and Cs-corrected Scanning TEM (STEM). To make a comparison, we also studied the effect of insulating oxides and asymmetric oxide electrodes on PTO films. $SrRuO_3$ (SRO) and $La_{0.7}Sr_{0.3}MnO_3$ (LSMO) were chosen as oxide electrodes because of their similar perovskite structures which are

a)Author to whom correspondence should be addressed: ylzhu@imr.ac.cn

beneficial for layer-by-layer film growth. It is noted that conducting SRO transforms into insulating at layer thicknesses below 2–4 unit cells.[17,18] For LSMO, the reported critical thickness of metallic behavior is about 3.2 or 4 nm.[19] The thicknesses of SRO and LSMO electrodes chosen here are in the range of 3.5–5 nm and 5–7 nm, so that they both are conductive.

The cross-sectional samples were prepared by the conventional method: first slicing, then gluing face to face, next grinding, dimpling, and finally ion milling.[20] High angle angular dark field (HAADF)-STEM imaging was conducted using a Titan Cubed 60–300 kV microscope (FEI) with the beam convergence angle of 25 mrad and the collection angle ranging from 50 mrad to 250 mrad. At room temperature, the bulk $PbTiO_3$ has a tetragonal structure with its lattice parameters: $a = b = 3.900$ Å and $c = 4.148$ Å, as shown in Fig. 1(a).

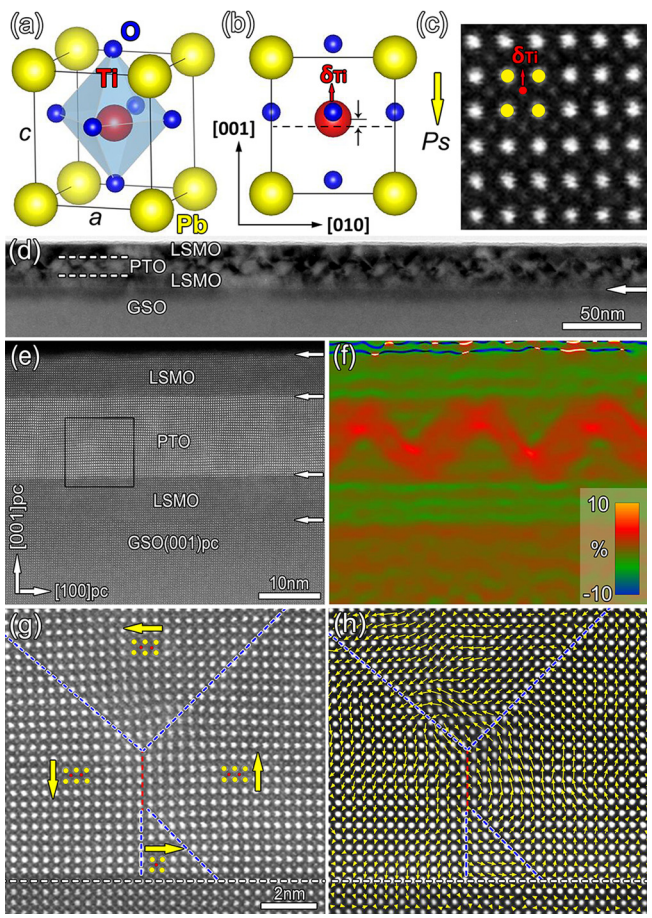

FIG. 1. Large scale periodic arrays of flux-closure domains in a 12 nm PTO film with top and bottom LSMO (7 nm) oxide electrodes grown on the GSO (110) substrate. (a) A schematic perspective view of the unit cell of PTO. (b) Projection of the unit cell along the [100] direction showing Ti^{4+} ion displacement (δ_{Ti}). (c) The HAADF-STEM image of the PTO crystal recorded with the incident electron beam parallel to the $[100]_{pc}$ direction. The positions of Pb^{2+} columns appear brighter than those of the Ti^{4+} columns. (d) Cross-sectional bright field TEM image and (e) High-resolution HAADF-STEM image of the film. The interfaces are marked by white arrows in (e). (f) Out-of-plane strain (ε_{yy}) map of (e) extracted via the GPA analysis. (g) Atomically resolved HAADF-STEM images of the areas labeled by the black rectangle in (e). (h) Superposition of reversed δ_{Ti} vectors with the atomic mapping. Yellow arrows denote reversed δ_{Ti} vectors which are consistent with the spontaneous polarization direction of PTO. The blue, red, and white dashed lines indicate 90°, 180° domain walls, and the interface between PTO and bottom LSMO, respectively. The scheme of arrows and lines is used in the following figures.

Both the O^{2-} and Ti^{4+} columns have displacements from the center of the Pb^{2+} tetragonal cell along the [001] axes, but the displacements of O^{2-} columns are larger [Fig. 1(b)]. As a consequence, the center of the positive and negative charges separate from each other, which causes an electrical dipole pointing from negative charge center to the positive charge center. Thus, the polarization directions of PTO unit cells can be determined to be opposite to the shifts of Ti^{4+} denoted as δ_{Ti} in Figs. 1(b) and 1(c). This method is widely approved and has been used in many publications.[8,9,21] The Pb^{2+} columns appear brighter than Ti^{4+} columns in the HAADF-STEM images since the intensity of the atom columns is approximately proportional to Z^2, where Z is the atomic number, in this imaging mode as shown in Fig. 1(c). For simplicity, the orientations marked below with subscript "pc" all represent pseudo-cubic perovskite, and the $[001]_{pc}$ orientation indicates the out-of-plane direction which is the direction of the film growth. Figures 1(d)–1(f) shows a 12 nm PTO film with top and bottom LSMO (7 nm) oxide electrodes layers grown on the GSO substrate. Figure 1(d) is a cross-sectional bright field TEM image of the film, from which it can be seen that the interfaces of film/substrate and PTO/LSMO are flat as denoted by the white arrow and white dashed lines, respectively. Contrast fluctuation can be identified in the PTO layer, indicating the existence of the domain pattern. Figure 1(e) displays a low magnification high-resolution HAADF-STEM image showing the domain pattern. The interfaces indicated by white arrows in Fig. 1(e) are atomically flat, and there is no signal of interdiffusion. Figure 1(f) shows the corresponding out-of-plane strain (ε_{yy}) map of Fig. 1(e) extracted via the geometric phase analysis (GPA).[22–24] According to the domain definition of tetragonal PTO,[25] the inhomogeneous out-of-plane strain distribution indicates that different domains exist here. As shown in Fig. 1(f), the out-of-plane strain in the substrate area is set to be zero; then, areas in red color with a large out-of-plane lattice parameter represent *c* domains, while *a* domains are the areas in green with a small out-of-plane lattice parameter. The *c* domains form a one-dimensional periodic sinusoidal array, whereas the *a* domains with triangular configurations present another periodic array. Figure 1(g) is the atomically resolved HAADF-STEM image of the area labeled with a black rectangle in Fig. 1(e). Figure 1(h) shows the corresponding mapping of reversed δ_{Ti} vectors. Yellow arrows denote reversed δ_{Ti} vectors which are consistent with the spontaneous polarization directions of PTO. As shown in Figs. 1(g) and 1(h), it is obvious that a flux-closure domain exists, while the small *a* domain near the interface of PTO/LSMO, which is hardly observed in strain mapping, is clearly seen here. The flux-closure domain is composed of two 3-fold vertices connected by a 180° domain wall (red dashed line). Such a configuration was predicted by Srolovitz and Scott in 1986 for ferroelectrics[26] and has been observed experimentally in PTO layers of PTO/STO multilayers by Tang *et al.* recently.[8] It is noted that the lower part of the three-fold vertex domain appears with two 90° domain walls with asymmetric distributing, contrasting with the symmetric distributions of two 90° domain walls around one 180° domain wall in flux-closure domains in PTO layers contacting with STO layers.[8] Combined with the strain

mapping [Fig. 1(f)], the flux-closure domain displays a periodic arrangement in the PTO layer. The period of flux-closure is measured to be about 19 nm and agrees with the rule proposed by Tang *et al.*[8]

Figure 2 shows a 12 nm PTO film with top and bottom SRO (3.5 nm) oxide electrode layers grown on the GSO substrate. Figure 2(a) is a cross-sectional dark field TEM image of the film, while the interfaces are labeled with white arrow and dashed lines. From Fig. 2(a), contrast fluctuation similar to Fig. 1(d) is observed which may indicate that a similar domain pattern appears in the PTO layer between the SRO electrode layers. In order to confirm this deduction, a high-resolution HAADF-STEM image, the corresponding out-of-plane strain (ε_{yy}) map, and an atomically resolved image of labeled area are shown in Figs. 2(b)–2(d). From Fig. 2(b), the interfaces indicated by white arrows are also flat with only one unit cell fluctuation. Figures 2(c)–2(e) shows the similar flux-closure domain as discussed previously meanwhile this flux-closure domain also gives rise to a periodic array with the expected period of about 17 nm. To confirm and also make a comparison with the flux-closure domain patterns in insulating conditions, a (STO(5 nm)/PTO(10 nm))$_2$ multilayered film grown on the GSO substrate was prepared and shown in Fig. 3. The contrast in the cross-sectional bright field TEM image [Fig. 3(a)] and the strain distribution in the out-of-plane strain (ε_{yy}) map [Fig. 3(c)] both manifest periodic flux-closure arrays with a period of about 15 nm in the two PTO layers under the insulated boundary condition.

The results above indicate that the flux-closure domains can exist and form periodic arrays in PTO layers between insulating STO layers and also between conductive LSMO or SRO electrode layers under the scandate substrate constraints. The result for insulating STO layers is similar to the

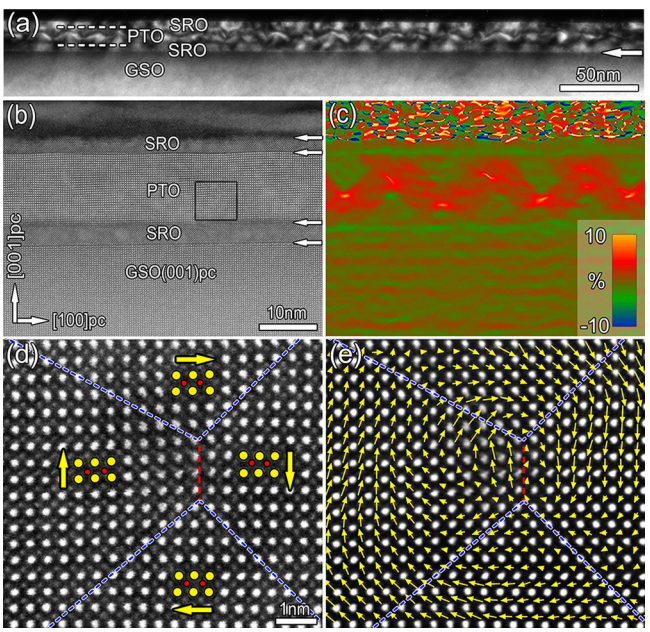

FIG. 2. Large scale periodic flux-closure arrays in a 12 nm PTO film with top and bottom SRO (3.5 nm) oxide electrodes grown on the GSO (110) substrate. (a)–(c) The cross-sectional dark field TEM image, high-resolution HAADF-STEM image, and corresponding out-of-plane strain (ε_{yy}) map of the film. (d) Atomically resolved HAADF-STEM images of the areas labeled by the black rectangle in (b). (e) Superposition of reversed δ_{Ti} vectors with the atomic mapping.

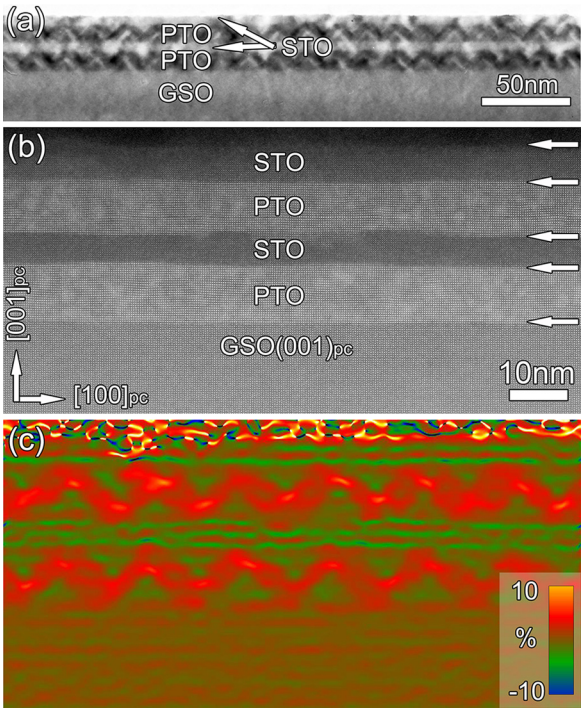

FIG. 3. Large scale periodic flux-closure arrays in PTO layers of a (STO(5 nm)/PTO(10 nm))$_2$ multilayered film grown on the GSO (110) substrate. (a)–(c) Cross-sectional bright field TEM images, high-resolution HAADF-STEM image, and corresponding out-of-plane strain (ε_{yy}) map of the multilayered film.

previous studies because of the maximized depolarization field and the appropriate epitaxial strain supplied by the substrate.[8–11] The formation of flux-closure domains in PTO layers sandwiched by symmetric LSMO or SRO electrodes can be understood as follows: It is well-known that the equilibrium domain patterns are formed as a balance of various energies, in particular, the electrostatic energy, elastic energy, and domain wall energy. If the depolarization field is completely compensated, the equilibrium domain patterns should be *c*/*a*/*c*/*a*… for PTO films grown on GSO substrates as proposed by Speck and Pompe.[27] Theoretical calculations indicate that a full screening occurs only upon ferroelectric thin films with suitable thickness and the electrodes with small screening lengths (a fraction of an Angstrom).[15,28] The screening lengths of LSMO and SRO are about 3 Å and 6 Å, respectively, which are approximately 10 times larger than those of metal electrodes such as aluminum electrodes (0.45 Å).[29,30] Due to the relatively large screening length of oxide electrodes, it is highly possible that the screening effect is incomplete in the present study. Therefore, the flux-closure domains can be stabilized in the PTO layers with the symmetric LSMO or SRO electrodes by the partially screened depolarization field. In particular, Vorotiahin *et al.*[31] has shown that a decrease in the screening length leads to an increase in the period of the domain structure, which may explain the slight difference in the periods of flux-closure domains of the PTO films with symmetric electrodes of LSMO (19 nm) and SRO (17 nm).

To further explore the role of electrode, a 12 nm PTO layer with asymmetric top LSMO (5 nm) and bottom SRO (5 nm) electrode layers was grown on the GSO substrate, and

the result was shown in Fig. 4. Figure 4(a) displays a cross-sectional bright field TEM image of the film showing the contrast fluctuation in the PTO layer which is apparently different from that in Figs. 1(d), 2(a), and 3(a). Some areas with bright and dark contrast appear in the PTO layer probably from *a*/*c* domain distributions which are commonly observed in ferroelectric films.[7,32] It means the asymmetric electrode configuration greatly modifies the domain structures in the PTO layer. Figure 4(b) is the high-resolution HAADF-STEM image of the film in which the interfaces are flat as denoted by white arrows. To demonstrate the domain pattern clearly, the corresponding out-of-plane strain (ε_{yy}) map is shown in Fig. 4(c), in which red areas in the PTO layer represent *c* domains, and green areas represent *a* domains. The pseudo perovskite lattice parameter of GSO substrate is 3.967 Å between *a* and *c* lattice parameters of the PTO bulk. Considering the absence of misfit dislocation at interfaces, the in-plane lattice parameter of the SRO layer adopts that of GSO, which exerts a tensile stress upon the PTO layer to facilitate formation of domains. Figure 4(d) gives the magnified images of the areas labeled with a black rectangle in Fig. 4(b). The spontaneous polarization directions are signified by yellow arrows, while the interface of LSMO/PTO and 90° domain walls are marked by white and blue dashed lines, respectively. Figure 4(e) is the superposition of reversed δ_{Ti} vectors with the atomic mapping. It is clear that the 90° domain walls are uncharged with head-to-tail polarizations whose energies are usually lower than the charged domain walls.

Although both are under conductive boundary conditions, the domain configuration of the PTO layer with the top-LSMO and bottom-SRO electrodes changes to *a*/*c* domains (Fig. 4) instead of periodic flux-closure arrays in the PTO layers between symmetric electrodes (Figs. 1 and 2). The

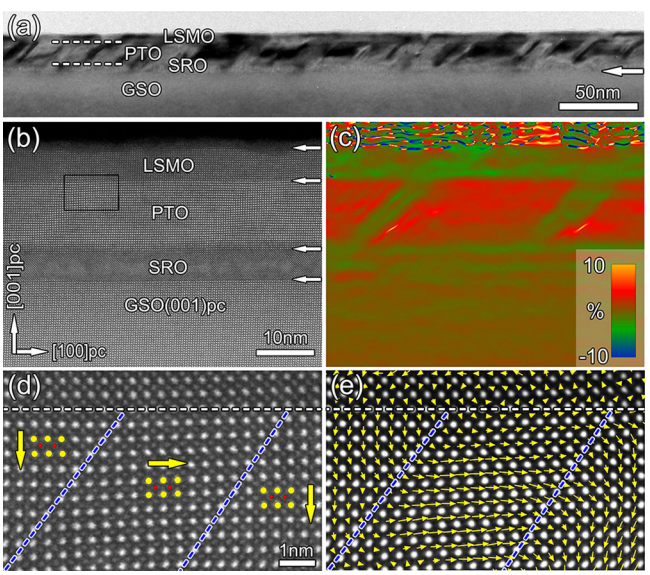

FIG. 4. *a*/*c* domains in a 12 nm PTO film with top LSMO (5 nm) and bottom SRO (5 nm) oxide electrode layers grown on the GSO (110) substrate. (a)–(c) Cross-sectional bright field TEM image, high-resolution HAADF-STEM image, and corresponding out-of-plane strain (ε_{yy}) map of the film. (d) Atomically resolved HAADF-STEM images of the areas labeled by the black rectangle in (b). (e) Superposition of reversed δ_{Ti} vectors with the atomic mapping.

annihilation of flux-closure domains may be relevant to the asymmetry between the top and bottom boundary conditions. Since the electrostatic fields decay exponentially with the distance from the film surface,[33] asymmetric electrodes can affect the domain structure when the period of the domains is comparable with the film thickness. In our experiment, the periods of flux-closure domains are about 15–19 nm, while the film thicknesses are 10 or 12 nm. Thus, it is reasonable to discuss the effect of asymmetric electrodes on the domain structure. As pointed out previously, the asymmetric electrical boundary conditions can indeed affect ferroelectric polarization, domain morphology, and physical properties of the ferroelectric film.[11,12,15,34] In the work of Peters *et al.*,[12] the asymmetric screening to the depolarization field was used to explain the asymmetry of polarization states in 180° domains and the formation of flux-closure domains. However, the asymmetric screening of the depolarization field should not result in the difference in two domains separated by a 180° domain wall, since the magnitudes of depolarization fields in the two domains are exactly the same.[15] Furthermore, our results indicate that the asymmetric electrodes tend to favor the formation of *a*/*c* domains with the same direction of spontaneous polarization in the *c* domain (away from LSMO electrode), as shown in Fig. 4. A similar result that the spontaneous polarization pointing away from the LSMO layer has been observed in the PZT layer between top LSMO and bottom SRO electrodes.[35] Therefore, the evolution of flux-closure domains into *a*/*c* domains is driven by the preference of the directions of out-of-plane spontaneous polarizations. Previous studies evidence that electrodes can affect the polarization states in ferroelectric films by their difference work functions.[36,37] When the top and bottom layers have different work functions, such as LSMO and SRO, it will result in a potential difference between the top and bottom surfaces of the PTO layers.[38] Thus, the direction of spontaneous polarization in the *c* domain is away from the LSMO electrode in our experiment because LSMO has a larger work function than SRO.[39] On the other hand, according to the theory proposed by Morozovska *et al.*, the conductivity types of electrodes should affect the final screening effect for a ferroelectric layer, and only the polarization with the direction opposite to that of the built-in electric field can be effectively screened when two thin electrodes with different conductivity types are applied.[40] The LSMO/PTO/SRO multilayer could be considered as a semiconductor/ferroelectric/metal model, since LSMO is a p-type semiconductor,[41,42] and SRO is metallic.[43] Thus, there exists an intrinsic built-in electric field which helps to stabilize the polarization with the reversed direction (away from LSMO). To further verify this, we also switched the positions of these two oxide electrodes and prepared SRO/PTO/LSMO/GSO film systems. It is found that the polarization in the PTO layer behaves the same and points away from LSMO (the results are not shown here), which indicates the intrinsic nature of the built-in field in these systems.

In summary, PTO films with symmetric and asymmetric top and bottom oxide electrodes were deposited on GSO substrates by the PLD technique. Cs-corrected TEM demonstrates that periodic arrays of flux-closure domains can form

in PTO layers with symmetric electrodes due to incomplete screening to the depolarization fields; whereas *a*/*c* domains form when asymmetric electrodes are applied probably caused by the differences in both work functions and conductivity types of the two oxide electrodes. The structural characteristics (such as period/thickness ratio) of these flux-closure arrays are nearly the same as those in PTO films sandwiched by insulating oxides. The present results are expected to give further understanding of the nature of topological domain formation and may also assist the development of the vortex-type structures' applications such as high-density memories and high-performance energy-harvesting devices.

This work was supported by the National Natural Science Foundation of China (Grant Nos. 51571197, 51401212, 51231007, 51501194 and 51671194), National Basic Research Program of China (2014CB921002), and the Key Research Program of Frontier Sciences CAS (QYZDJ-SSW-JSC010). Y.L.T. acknowledges the IMR SYNL-T.S. Kê Research Fellowship and the Youth Innovation Promotion Association CAS (Grant No. 2016177). We are grateful to Mr. B. Wu and Mr. L. X. Yang of this lab for their technical support on the Titan platform of G^2 60-300 kV aberration-corrected scanning transmission electron microscope.

[1]J. F. Scott and C. A. Paz de Araujo, Science **246**, 1400 (1989).
[2]J. Gao, Y. Wang, Y. Liu, X. Hu, X. Ke, L. Zhong, Y. He, and X. Ren, Sci. Rep. **7**, 40916 (2017).
[3]D. Pantel, H. Lu, S. Goetze, P. Werner, D. J. Kim, A. Gruverman, D. Hesse, and M. Alexe, Appl. Phys. Lett. **100**, 232902 (2012).
[4]L. W. Martin, Y. H. Chu, and R. Ramesh, Mater. Sci. Eng. R **68**, 89 (2010).
[5]Z. Y. Chen, Y. X. Su, Z. D. Zhou, L. S. Lei, and C. P. Yang, AIP Adv. **6**, 055207 (2016).
[6]I. I. Naumov, L. Bellaiche, and H. X. Fu, Nature **432**, 737 (2004).
[7]G. Catalan, A. Lubk, A. H. G. Vlooswijk, E. Snoeck, C. Magen, A. Janssens, G. Rispens, G. Rijnders, D. H. A. Blank, and B. Noheda, Nat. Mater. **10**, 963 (2011).
[8]Y. L. Tang, Y. L. Zhu, X. L. Ma, A. Y. Borisevich, A. N. Morozovska, E. A. Eliseev, W. Y. Wang, Y. J. Wang, Y. B. Xu, Z. D. Zhang, and S. J. Pennycook, Science **348**, 547 (2015).
[9]A. K. Yadav, C. T. Nelson, S. L. Hsu, Z. Hong, J. D. Clarkson, C. M. Schlepueetz, A. R. Damodaran, P. Shafer, E. Arenholz, L. R. Dedon, D. Chen, A. Vishwanath, A. M. Minor, L. Q. Chen, J. F. Scott, L. W. Martin, and R. Ramesh, Nature **530**, 198 (2016).
[10]Z. D. Zhou and D. Y. Wu, AIP Adv. **5**, 107206 (2015).
[11]S. Prosandeev and L. Bellaiche, Phys. Rev. B **75**, 172109 (2007).
[12]J. J. P. Peters, G. Apachitei, R. Beanland, M. Alexe, and A. M. Sanchez, Nat. Commun. **7**, 13484 (2016).
[13]C. T. Nelson, B. Winchester, Y. Zhang, S.-J. Kim, A. Melville, C. Adamo, C. M. Folkman, S.-H. Baek, C.-B. Eom, D. G. Schlom, L.-Q. Chen, and X. Pan, Nano Lett. **11**, 828 (2011).
[14]M. F. Chisholm, W. Luo, M. P. Oxley, S. T. Pantelides, and H. N. Lee, Phys. Rev. Lett. **105**, 197602 (2010).
[15]M. Y. Zhuravlev, R. F. Sabirianov, S. S. Jaswal, and E. Y. Tsymbal, Phys. Rev. Lett. **94**, 246802 (2005).
[16]M. Dawber, P. Chandra, P. B. Littlewood, and J. F. Scott, J. Phys.: Condens. Matter **15**, L393 (2003).
[17]J. Xia, W. Siemons, G. Koster, M. R. Beasley, and A. Kapitulnik, Phys. Rev. B **79**, 140407 (2009).
[18]Y. J. Chang, C. H. Kim, S. H. Phark, Y. S. Kim, J. Yu, and T. W. Noh, Phys. Rev. Lett. **103**, 057201 (2009).
[19]M. Huijben, L. W. Martin, Y. H. Chu, M. B. Holcomb, P. Yu, G. Rijnders, D. H. A. Blank, and R. Ramesh, Phys. Rev. B **78**, 094413 (2008).
[20]S. Li, Y. L. Zhu, Y. L. Tang, Y. Liu, S. R. Zhang, Y. J. Wang, and X. L. Ma, Acta Mater. **131**, 123 (2017).
[21]S. M. Anthony and S. Granick, Langmuir **25**, 8152 (2009).
[22]M. J. Hytch, E. Snoeck, and R. Kilaas, Ultramicroscopy **74**, 131 (1998).
[23]Y. L. Tang, Y. L. Zhu, and X. L. Man, Ultramicroscopy **160**, 57 (2016).
[24]Y. Liu, Y.-L. Tang, Y.-L. Zhu, W.-Y. Wang, and X.-L. Ma, Adv. Mater. Interfaces **3**, 1600342 (2016).
[25]A. L. Roytburd, S. P. Alpay, L. A. Bendersky, V. Nagarajan, and R. Ramesh, J. Appl. Phys. **89**, 553 (2001).
[26]D. J. Srolovitz and J. F. Scott, Phys. Rev. B **34**, 1815 (1986).
[27]J. S. Speck and W. Pompe, J. Appl. Phys. **76**, 466 (1994).
[28]J. Bardeen, Phys. Rev. **71**, 717 (1947).
[29]J. Junquera and P. Ghosez, Nature **422**, 506 (2003).
[30]X. Hong, A. Posadas, and C. H. Ahn, Appl. Phys. Lett. **86**, 142501 (2005).
[31]I. S. Vorotiahin, E. A. Eliseev, Q. Li, S. V. Kalinin, Y. A. Genenko, and A. N. Morozovska, "Tuning the polar states of ferroelectric films via surface charges and flexoelectricity," preprint arXiv:1704.00136 (2017).
[32]A. H. G. Vlooswijk, B. Noheda, G. Catalan, A. Janssens, B. Barcones, G. Rijnders, D. H. A. Blank, S. Venkatesan, B. Kooi, and J. T. M. de Hosson, Appl. Phys. Lett. **91**, 112901 (2007).
[33]L. E. Cross, A. K. Tagantsev, and J. Fousek, *Domains in Ferroic Crystals and Thin Films* (Springer, New York, 2010).
[34]Q. Yang, J. X. Cao, Y. Ma, Y. C. Zhou, X. J. Lou, and J. Yang, J. Appl. Phys. **114**, 034109 (2013).
[35]S. R. Spurgeon, J. D. Sloppy, D. M. Kepaptsoglou, P. V. Balachandran, S. Nejati, J. Karthik, A. R. Damodaran, C. L. Johnson, H. Ambaye, R. Goyette, V. Lauter, Q. M. Ramasse, J. C. Idrobo, K. K. S. Lau, S. E. Lofland, Jr., J. M. Rondinelli, L. W. Martin, and M. L. Taheri, ACS Nano **8**, 894 (2014).
[36]L. Pintilie, I. Vrejoiu, D. Hesse, and M. Alexe, J. Appl. Phys. **104**, 114101 (2008).
[37]S. Na, A. M. Kolpak, and A. M. Rappe, Phys. Rev. B **72**, 020101 (2005).
[38]C. Yoshida, A. Yoshida, and H. Tamura, Appl. Phys. Lett. **75**, 1449 (1999).
[39]R. Jacobs, J. Booske, and D. Morgan, Adv. Funct. Mater. **26**, 5471 (2016).
[40]A. N. Morozovska, E. A. Eliseev, S. V. Svechnikov, A. D. Krutov, V. Y. Shur, A. Y. Borisevich, P. Maksymovych, and S. V. Kalinin, Phys. Rev. B **81**, 205308 (2010).
[41]T. Muramatsu, Y. Muraoka, and Z. Hiroi, Solid State Commun. **132**, 351 (2004).
[42]S. Chattopadhyay, J. Panda, and T. K. Nath, J. Appl. Phys. **113**, 194501 (2013).
[43]G. Koster, L. Klein, W. Siemons, G. Rijnders, J. S. Dodge, C.-B. Eom, D. H. A. Blank, and M. R. Beasley, Rev. Mod. Phys. **84**, 253 (2012).